

# Nanoscale

Accepted Manuscript



This is an *Accepted Manuscript*, which has been through the Royal Society of Chemistry peer review process and has been accepted for publication.

*Accepted Manuscripts* are published online shortly after acceptance, before technical editing, formatting and proof reading. Using this free service, authors can make their results available to the community, in citable form, before we publish the edited article. We will replace this *Accepted Manuscript* with the edited and formatted *Advance Article* as soon as it is available.

You can find more information about *Accepted Manuscripts* in the [Information for Authors](#).

Please note that technical editing may introduce minor changes to the text and/or graphics, which may alter content. The journal's standard [Terms & Conditions](#) and the [Ethical guidelines](#) still apply. In no event shall the Royal Society of Chemistry be held responsible for any errors or omissions in this *Accepted Manuscript* or any consequences arising from the use of any information it contains.

## ARTICLE

# A Highly Sensitive Nanoscale pH-sensor using Au Nanoparticles Linked by a Multifunctional Raman-active Reporter Molecule

Cite this: DOI: 10.1039/x0xx00000x

Latevi S. Lawson<sup>a,b</sup>, James W. Chan<sup>ac</sup>, and Thomas Huser<sup>a,d</sup>Received 00th January 2012,  
Accepted 00th January 2012

DOI: 10.1039/x0xx00000x

[www.rsc.org/](http://www.rsc.org/)

**Abstract:** Chemical sensing on the nanoscale has been breaking new ground since the discovery of surface enhanced Raman scattering (SERS). For nanoparticles, controlled particle aggregation is necessary to achieve the largest SERS enhancements. Therefore, aggregating agents such as salts or linker molecules are used in conjunction with chemically sensitive reporters in order to develop robust environmentally sensitive SERS probes. While salt-induced colloidal nanosphere aggregates have produced robust SERS signals, their variability in aggregate size contributes significantly to poor SERS signal reproducibility, which can complicate their use in *in vitro* cellular studies. Such systems often also lack reproducibility in spectral measurements between different nanoparticle clusters. Preaggregation of colloids via linkers followed by surface functionalization with reporter molecules results in the linker occupying valuable SERS hotspot volume which could otherwise be utilized by additional reporter molecules. Ideally, both functionalities should be obtained from a single molecule. Here, we report the use of 3,5-dimercaptobenzoic acid, a single multifunctional molecule that creates SERS hotspots via the controlled aggregation of nanoparticles, and also reports pH values. We show that 3,5-dimercaptobenzoic acid bound to Au nanospheres results in an excellent pH nanoprobe, producing very robust, and highly reproducible SERS signals that can report pH across the entire physiological range with excellent pH resolution. To demonstrate the efficacy of our novel pH reporters, these probes were also used to image both the particle and pH distribution in the cytoplasm of human induced pluripotent stem cells (hiPSCs).

## 1. Introduction

Surface enhanced Raman scattering (SERS) is increasingly gaining applications in the analysis and imaging of biological or chemical processes that occur at the cellular and tissue level. SERS has been reported to yield as much as 15 orders of magnitude greater signal than normal Raman scattering, and therefore allows for chemically specific imaging and spectroscopy that can readily compete with strong fluorescence signals. Unlike fluorophores, SERS probes are not prone to photobleaching, thus making them ideal candidates for long term biological studies.<sup>1-4</sup> Also, spectral overlap is reduced because Raman bands are narrow, and thus SERS particles are interesting probes for multiplexed imaging<sup>5</sup>. Since many biological processes, such as elevated metabolic activity, are mitigated by pH differentials, SERS probes that are responsive

to pH changes are of significant interest and have demonstrated success in monitoring pH values *in vitro*. Typically, these pH-sensitive probes consist of a weak acid as a reporter moiety and gold (Au) or silver (Ag) nanoparticles (NPs) as the enhancing, surface-plasmon-resonant metal scaffold. Since SERS enhancements are greatest at the point of contact between nanostructures, NPs are typically induced to aggregate in the presence of a reporter molecule by changing the ionic strength of the solution; this is usually achieved by adding salts or by decreasing the pH of the solution. Although ionic strength-induced aggregation produces very intense SERS signals and has been very successful, the Raman modes indicative of pH changes can vary non-uniformly due to differences in the size of aggregates, the distance between constituents within an aggregate, and the resulting effects e.g. on the electric double-layer around each NP within an aggregate. These effects result in variations in the peak ratios of their respective SERS spectra

and lead to significant variation in the pH value calculated from these peak ratios. Chemical imaging and/or sensing via SERS has most commonly utilized the presence or absence of spectral bands as a characteristic means for determining pH values and the peak ratio of the chemically sensitive modes as quantifying means. Therefore, ways by which spectral and signal strength fluctuations can be reduced will translate into better quantifying pH resolution and are sought after and welcomed by the scientific community. Several techniques, including probe encapsulation, and/or using metal scaffolds such as silica-core Au-shelled (SCAS) NPs or hollow gold NPs (HGPN) have shown great success in producing SERS signal with lower spectral deviation and higher overall reproducibility.<sup>6-8</sup> These improvements have translated into our ability to now quantify pH changes with biologically relevant pH resolution. HGPN and SCAS scaffolds are also able to produce measurable SERS signals that emanate from reporter molecules anchored to a single colloid as opposed to dimerized colloids, and minimize the need for colloidal aggregation<sup>8</sup>. Even though scaffold designs have improved the detection of chemical indicators, such as pH, they are more costly in terms of time, knowhow, and research funds, and - regardless of the colloidal design, it is by now well established that the greatest SERS signals occur when a reporter molecule finds itself right at the junction of nano-structures and/or particles.<sup>9-13</sup> To improve signal strength, techniques that facilitate the formation of stable, dimerized metal colloids are being developed and are highly desired.<sup>14-16</sup> Controlled nanoparticle linking has been explored with success by Braun et. al.<sup>17</sup> In their 2009 paper, nanoparticles are prelinked with a tethering molecule before a reporter is added. An equally impressive collaboration Laurence et. al. showed that silver (Ag) nanoparticles tethered together with the linker moiety 4-aminobenzenethiol (ABT) yield more SERS active and intense species than untethered nanospheres.<sup>18</sup> Brauns' approach was also used successfully to measure pH. Using Ag colloids prelinked with 1,6-diaminohexane followed by functionalization with a SERS pH reporter, 4-mercaptobenzoic acid (4-MBA), Braun created a bright SERS tags capable of pH sensing.<sup>16</sup> Like other measurements conducted with 4-MBA (e.g. our initial intracellular SERS pH report from 2004<sup>19</sup>), this method produced SERS signal strengths that could successfully compete with fluorescence.<sup>12, 16, 19-21</sup> However, in this case it is the linker molecule that occupies the most robust SERS hot spots and not the actual pH reporter molecule. Also, hot spot volumes for the actual reporter molecules are reduced since the linker molecule is also occupying them. Therefore, the maximum SERS intensity of the pH reporter is typically not realized. Thus, it is important for the next generation of environmentally-responsive SERS probes to perform as much from the signal-enhancing hot spot sites as possible. In this paper we describe the synthesis and characterization of 3,5-dimercaptobenzoic acid (3,5-DMBA) as a disulfide pH reporter that can both cause size-selective AuNP aggregate formation (thus creating its own hotspot to occupy) and also report pH with excellent pH resolution via SERS without any additional inducers of aggregation. We then used these pH probes to determine intracellular pH levels inside human induced pluripotent stem cells (hiPSCs) and to construct a pH map of the cell's interior. We believe that in the future we will be able to monitor changes in the distribution and dynamics of pH levels in differentiating cells, which in turn will help to mechanistically characterize the process of stem cell differentiation. We also believe that this will serve as a model for a new generation of SERS reporters designed to serve

multiple functions. Our reporter is designed to 1) cause selective colloidal aggregation, and therefore creates and occupies narrow interparticle junctions, 2) it turns out to be a powerful tool for imaging, 3) it can sense changes in pH, and 4) it can quantify changes in pH with high precision.

## 2. Experimental Materials and Methods

### 2.1. Raman spectroscopy system

The Raman spectra used to characterize the intermediates and final products during the synthesis of 3,5-DMBA were obtained on an Olympus IX71 inverted optical microscope. A diode-pumped solid-state laser (785nm, Crystalaser, Reno, NV) served as the excitation source. The laser is capable of yielding up to 32mW of laser power focused to a diffraction-limited spot at the sample after passing through a narrow-band clean-up filter, a neutral density filter, and a dichroic beam splitter. Raman spectra were obtained by coupling the Raman-scattered light into an Acton SpectraPro 2300i imaging spectrometer and utilizing a back-thinned Princeton Instruments Pixis 100BR CCD camera as multichannel detector.

SERS measurements on immobilized nanoparticles were acquired using a motorized optical microscope (iMic, Till Photonics, Munich, Germany). Image acquisition and coordination with Raman spectroscopy on this microscope was controlled by custom-written MATLAB software. A continuous Argon/Krypton ion laser (Innova 70c Spectrum, Coherent Inc., Santa Clara, CA) coupled into a single mode optical fiber and restricted to less than 1 mW output power provided the excitation source at 647 nm. At the sample the power of the diffraction-limited spot however was measured to be 300  $\mu$ W. The SERS spectra were again collected on a SpectraPro 2300i spectrometer (Acton Research) using a Pixis 100 CCD sensor (Princeton Instruments) directly attached to the iMic platform.

### 2.2. Spectral Analysis

In order to remove autofluorescence contributions from the spectra, the broadband background was subtracted from the spectral measurements after data collection using an automated background subtraction routine as first described by Lieber et al.<sup>22</sup> This allowed the the NP probe's pH-sensitivity in a flow cell to be standardized, which we could then use to compare them with SERS measurements taken within living cells. The automated subtraction routine was applied to all SERS spectra using a 6th order polynomial with 200 iterations, followed by normalizing the spectra to the 12a1  $\delta$ (ring) vibrational mode at roughly 1000  $\text{cm}^{-1}$ .<sup>22</sup> The background subtraction was performed on the entire spectral region, however after the background removal only the spectral region between 700 and 1800  $\text{cm}^{-1}$  was retained and is shown here. A median filter was also applied to smooth the data.

### 2.3. Synthesis of 3,5-Dimercaptobenzoic acid

3,5-Dimercaptobenzoic acid was synthesized in a three step protocol. A slight alteration in the procedure outlined by Corbett was used to synthesize the reporter molecule.<sup>23</sup> The modified protocol was used to synthesize another pH SERS reporter (2,5-Dimercaptobenzoic acid), which we utilized in a previous publication.<sup>24</sup> The synthesis and quantification of 3,5-DMBA is reported in more detail in the following section (Figure 1); we have also included the NMR and mass spectra of

the final compound in Figure S1-2 in the supplemental information file..

Under a nitrogen atmosphere methyl 3,5-dihydroxybenzoate (5.09 g, 30.3 mmol) was dissolved in 20mL anhydrous DMF. The solution was cooled to 0°C in an ice bath. Six portions of

### 2.3.1 Synthesis of Methyl 3,5-bis(dimethylcarbamothioxy)benzoate: (O-linked-3,5)

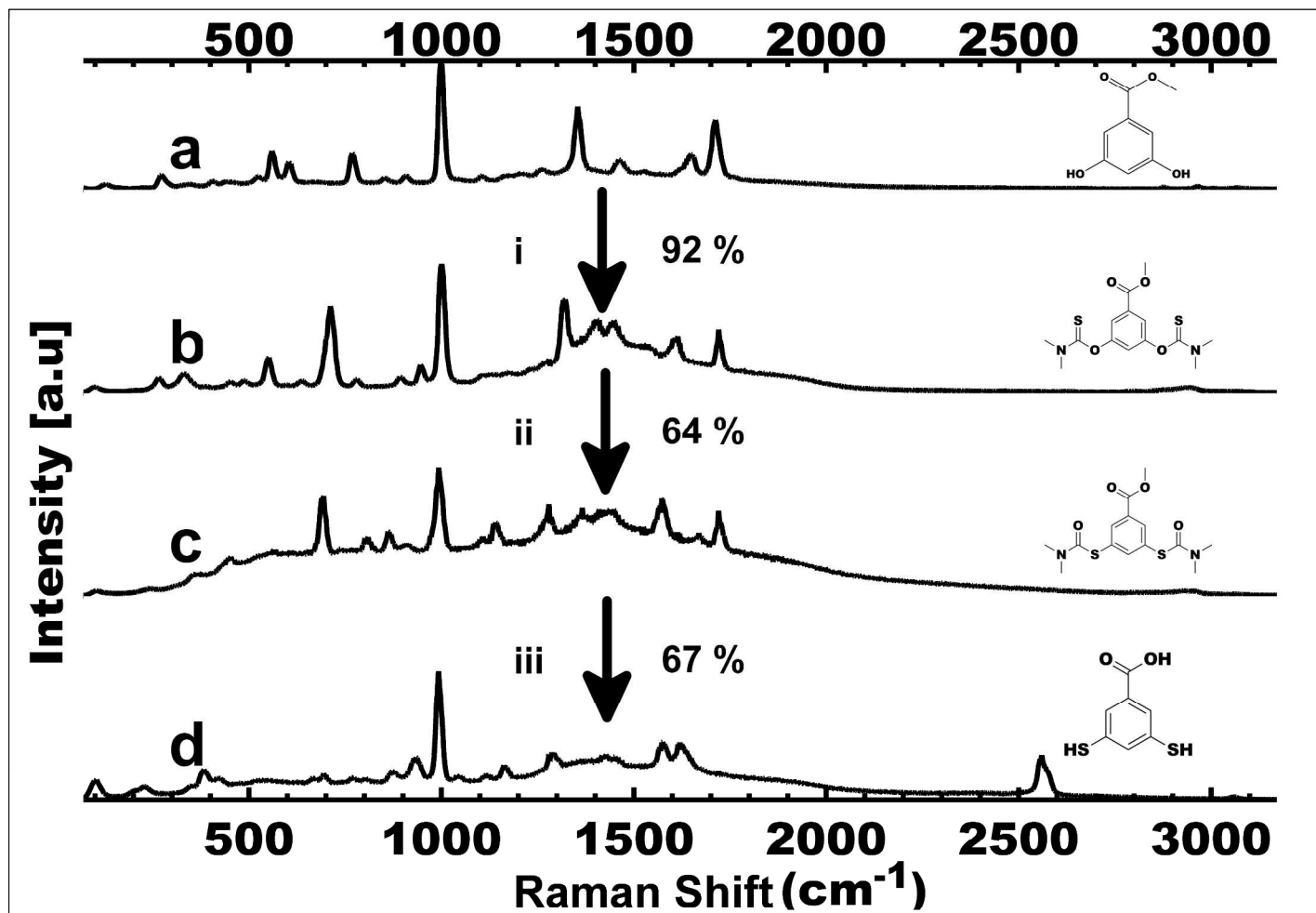


**Figure 1:** Synthesis of 3,5-dimercaptobenzoic acid; the synthesis is followed by analyzing the synthesis product at each step by Raman spectroscopy. Reaction i) At 0°C the starting material methyl 3,5-dihydroxybenzoate (a), 1,4-diazabicyclo[2.2.2]carbonyl (DABCO), and thiocarbonyl chloride were suspended and stirred vigorously in DMF. The mixture was then stirred at room temperature for 24 hrs. Reaction ii) The solution of thiocarbamate (b) was heated at temperatures between 230°C to 240°C for approximately 4 hrs in diphenyl ether (10ml diphenyl ether per gram of thiocarbamate) to produce product c. Reaction iii) In 175M of argon purged KOH in diethyleneglycol was used to suspend product "c." The suspension was then heated to 105°C for 30 minutes. After cooling to room temperature, argon-purged water was added to the reaction mix followed by the rapid addition of 10% HCl to yield the final product (d). The O-linked intermediate products (b) show Raman stretching vibrations at 1720cm<sup>-1</sup> and 2938cm<sup>-1</sup> indicating the presence of the ester and more sp<sup>3</sup> C-H functionalities, respectively. The S-linked intermediate products show vibrations at approximately 1669cm<sup>-1</sup> and 1720cm<sup>-1</sup> indicating the presence of the amide and ester functional groups, respectively. The acid products have peaks at roughly 1620cm<sup>-1</sup> and 2560cm<sup>-1</sup> delineating the carboxylic acid and thiol functional groups, respectively.

DABCO (13.3 g, ~4eq) were added to the solution. This was followed by adding 20ml of a 6M solution of N,N-dimethylthiocarbonyl chloride (~ 4eq) in DMF dropwise to the suspension over a 5 minute period at 4°C. The solution was allowed to warm to room temperature for roughly 24 hours. The mixture was poured into 200ml of water and stirred vigorously for 20 minutes until a precipitate had formed. The precipitate was collected via suction filtration and washed

extensively with H<sub>2</sub>O. The resulting 9.53g of crystals were placed under vacuum for 24 hours (92% yields).

### 2.3.2. Synthesis of Methyl 3,5-bis(dimethylcarbamoylthio)benzoate: (S-linked-3,5)

Under a nitrogen atmosphere, O-linked-3,5 (6.44 g, 18.8 mmol) was suspended in 67 ml of diphenyl ether. For roughly 5 hours the suspension was heated to 240°C. In an ambient environment the reaction mixture was permitted to cool to

roughly 35°C before being poured into 160 ml hexane. An ice bath was then employed, cooling the solution to 5°C. The ice bath was maintained until the maximum amount of badge crystals had formed (this took approximately 30 minutes). The crystals were collected via suction filtration, washed with copious amounts of warm hexane, and then placed under vacuum for 48hr (4.13g, 64% yield).

### 2.3.3. Synthesis of 3,5-dimercaptobenzoic acid: (3,5-DMBA).

A 1.75 M solution of KOH in diethylene glycol had been purged with argon gas for 4 hr. Under nitrogen gas methyl 3,5-bis(dimethylcarbamoylthio)benzoate (4.02 g, 11.17 mmol) was dissolved in the previously prepared KOH solution; this solution was then heated to approximately 105°C for about 45 minutes. After heating, the solution was permitted to cool to ambient temperature. The solution was poured into 500 ml of H<sub>2</sub>O that had been purged with argon gas for 2 hr, this was followed by the immediate addition of 50 ml of 12.1 normal HCl. The precipitate was collected using suction filtration, washed extensively with water, and then dried under vacuum for 48hr, yielding 1.61 g of dry product (69% yield). LC-MS: m/z: [M-H]<sup>-</sup> calculated: for C<sub>7</sub>H<sub>5</sub>O<sub>2</sub>S<sub>2</sub> was 185.2 found: 185.1; <sup>13</sup>C NMR (400 MHz, CD<sub>3</sub>OD): δ = 167.50, 134.01, 132.26, 131.95, 126.22; <sup>1</sup>H NMR (400 MHz, CD<sub>3</sub>OD): δ = 7.63(d,2H,2 x ArCH), 7.38 (t,1H, ArCH). Raman ν<sub>max</sub> = 2558.8 rel cm<sup>-1</sup> (br, S-H), 1624.2 rel cm<sup>-1</sup> (s, C=O), 1576.905 rel cm<sup>-1</sup> (s, C=C ring breathing stretch).

### 2.4. Gold Nanoparticle Synthesis

Gold (Au) nanoparticles (NPs) were synthesized via citrate reduction.<sup>25</sup> HAuCl<sub>4</sub> (24 mg) was dissolved in 50 mL of deionized water. The vigorously stirred solution was then heated until it began to boil. Approximately 5mL of a 1% solution of sodium citrate was added drop wise to the boiling solution. The solution continued to boil for 25 minutes and then rested overnight. The UV-VIS spectrum of the red-colored solution showed a maximum absorption peak at 530 nm. DLS measurements determined the colloids in solution had an average diameter of 35 nm (Figure 2). Dynamic light scattering (DLS) of colloidal particle solutions was conducted with a Zetatrac system (Microtrac), and a Varian 50 bio (Cary) spectrometer was used for UV-VIS measurements.

### 2.5. Human induced pluripotent stem cells (hiPSCs) culture and intracellular measurements.

HiPSCs (iPS-D19-9-T7, WiCell) were cultured under feeder-free condition in mTeSR (Stem Cell Technologies) on hESC-qualified matrigel (BD) and incubated at 37°C with 5% CO<sub>2</sub>. The cell culture medium was refreshed daily. Accutase (Innovative Cell Technologies) was used to dissociate the cells for passaging and plating for experiments.

SERS pH probe efficacy in vitro was evaluated with the hiPSCs by first plating the cells in a glass bottom Petri dish for 24 hrs before incubating with the SERS probes. We added 500 μL of the pH-probe (same colloidal gold solution we used for the calibration measurements, describe in the results) into the Petri dish. The hiPSC cells were then incubated for 2.5 hrs before measurements were performed. Just prior to the experiment the growth medium was replaced with phosphate buffer. A diffraction-limited laser spot was used in the local SERS

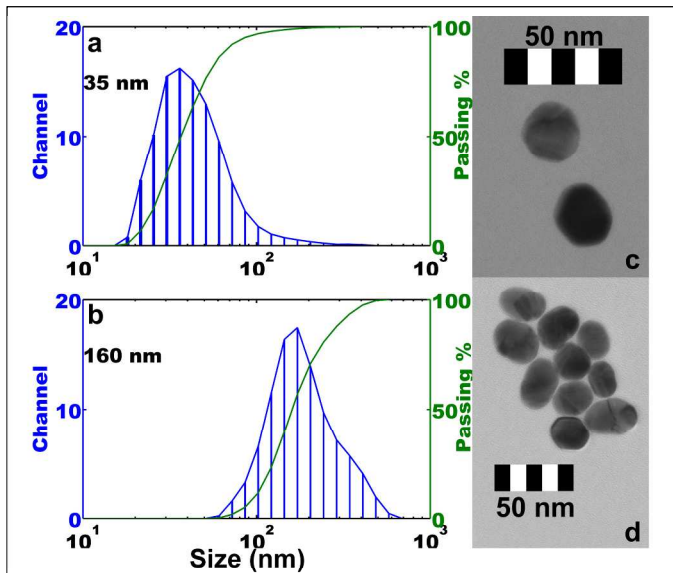


**Figure 2:** Dynamic light scattering (DLS) measurements of gold (Au) colloids before (a) and after (b) the addition of 3,5-dimercaptobenzoic acid (3,5-DMBA) show that our reporter molecule causes an increase in the average diameter of particles in the solution. The TEM images are of Au colloids before (c) and after (d) the addition of 3,5-DMBA. The TEM images indicate that increases in the average diameter is not caused by the amalgamation of colloids into one another.

measurements. The laser spot was moved to 25 equally spaced positions in both, the x and y direction until data were collected from each of the 625 different acquisition positions. This formed a 25 pixel x 25 pixel image grid that encompassed the entire stem cell. The z-position of the laser focus was adjusted to ensure that the cell's interior was being probed and imaged. SERS measurements were collected at each of the 625 points in the imaging area using a 1 second integration time per data point.

## 3. Results and Discussion

To the best of our knowledge, the synthesis of 3,5-DMBA has not yet been followed by Raman spectroscopy and therefore we highlight spectral features unique to each step in the synthesis pathway (Figure 1). We will be characterizing the ring vibrations with Wilson vibration assignments, using C<sub>2v</sub> symmetry for the tri-substituted benzene. All four compounds are 1,3,5-trisubstituted benzenes and therefore we observe the 12(a<sub>1</sub>) δ(ring) vibration characteristic for these compounds. At approximately 1720 cm<sup>-1</sup> the Raman spectra of the starting material and the two intermediates all exhibit a carbonyl stretching mode identifying a functional ester group.<sup>26-27</sup> This vibration is absent in the final product since the final product loses this ester group during the synthesis. The final product exhibits both, the ν(S-H) vibration at 2560 cm<sup>-1</sup> and the ν(C=O) stretching vibration at 1620 cm<sup>-1</sup> in its Raman spectrum. Aromatic carboxylic acids commonly have ν(C=O) vibrations at a lower wavenumber than non-aromatic carboxylic acids. Non-aromatic carboxylic acid vibrations are typically found at roughly 1700 cm<sup>-1</sup>. These vibrations are not seen in any of the preceding compounds indicating the successful synthesis of 3,5-DMBA. Unlike the o-linked intermediate the s-linked intermediate has a peak at roughly 1669 cm<sup>-1</sup>. This peak

indicates the presence of an amide carbonyl, and highlights a successful rearrangement outlined by Newman.<sup>28</sup> The mass-to-charge ratio of our final product was measured to be 185.1, while the calculated mass spectrum for the final product measures 185.2, signifying the successful synthesis of 3,5-DMBA. NMR measurements further confirm a successful synthesis. The carbon NMR (<sup>13</sup>C) spectrum identified the presence of five carbons ( $\delta = 167.50, 134.01, 132.26, 131.95, 126.22$ ) in the final compound. The chemical shifts for these carbons are similar to those mentioned by Corbett.<sup>23</sup> The proton NMR (<sup>1</sup>H) produced two distinctive chemical shifts, a single proton split into a triplet, and two equivalent protons split into a doublet. These splitting patterns are expected for a 1,3,5-substituted benzene ring where the 3 and 5 substituents are equivalent. The protons at the 2nd and 6th positions are equivalent and are split via “w-coupling” by the isolated proton in the 4th position. The triplet occurs because the isolated proton in the 4th position is split by equivalent protons in the 2nd and 6th positions.

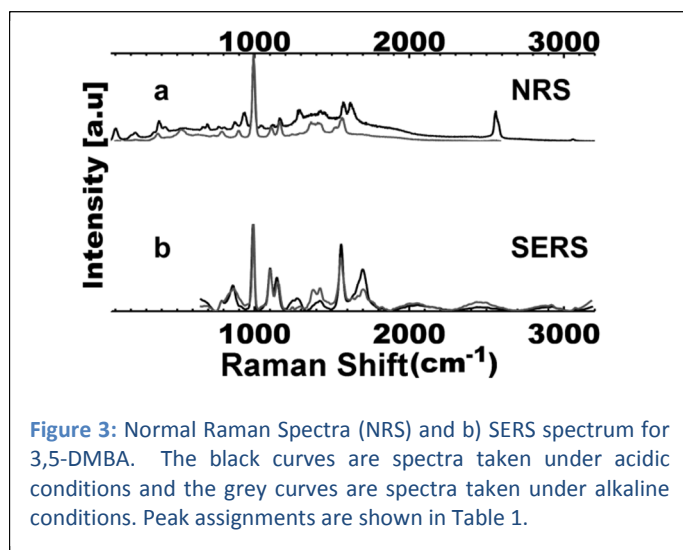


**Figure 3:** Normal Raman Spectra (NRS) and b) SERS spectrum for 3,5-DMBA. The black curves are spectra taken under acidic conditions and the grey curves are spectra taken under alkaline conditions. Peak assignments are shown in Table 1.

The concentration of the nanoparticle suspension directly after citrate reduction was determined by absorption measurements to be roughly  $2.8 \times 10^{11}$  particles/mL. The nanoparticle solution (500  $\mu$ L) was diluted with 1000  $\mu$ L of milli-Q water. UV-VIS measurements were taken of both the original and dilute colloidal solutions and both exhibited a maximum absorption at 530 nm. A single absorption maximum at 530 nm is characteristic of a colloidal gold solution with an average nanoparticle diameter of approximately 30 nm.<sup>29-30</sup> Dynamic light scattering (DLS) measurements taken of the solution confirmed the UV-VIS measurements. DLS measurements showed the mean diameter of colloids in solution to be 35 nm. The diluted NP solution was incubated with 5  $\mu$ L of a saturated solution of 3,5-DMBA dissolved in ethanol for 2 hours, ensuring that the nanoparticle surface was saturated with our linker molecule. It has been reported that, although the dominant binding mechanism for 1,3-benzendithiol (our linker molecule without the acid functional group) on Au colloids will cause the molecule to anchor both thiol endgroups to a single colloid, there is a secondary binding mechanism at high concentrations in which each thiol end group can occupy a different nanoparticle.<sup>31-32</sup> Although we cannot be entirely sure that our reporter molecule will mostly bridge between particles or bind to the same particle surface, it is clear that a concentration-dependent interparticle tethering mechanism

causes our pH-sensitive linker molecules to induce small, controlled aggregate growth. Using DLS and TEM the solution was compared to a control solution that had undergone the same procedure but lacking the reporter molecule (Figure 2). After exposure to 3,5-DMBA the mean diameter of the aggregates in the solution was measured with DLS and was determined to be 160 nm (Figure 2). The larger hydrodynamic radius indicates the formation of colloidal aggregates.<sup>33-35</sup> To further identify the aggregation characteristics, TEM micrographs were taken before and after the addition of our linker-reporter molecule (Figure 2). The size and shape of the nanoparticles remain consistent; therefore we concluded that our reporter molecule causes aggregate formation and did not reduce the metal. Although there is an excess of reporter molecules available, the equilibrium aggregate size is only approximately five times the colloidal diameter (originally  $\sim 30$  nm moving to  $\sim 160$  nm), indicating the formation of relatively small multimers across a large area (see the widefield TEM images of gold nanoparticles exposed to 3,5-DMBA in Figure S3), which are still suitable for applications in cellular studies. The selectivity of our approach could be further improved e.g. by nanoparticle size selection using gel chromatography. Interestingly, the equilibrium diameter of the aggregates is significantly larger than the equilibrium diameter produced by using 2,5-dimercaptobenzoic acid which we reported previously.<sup>24</sup>

**Table 1: Vibration Assignments for 3,5-DMBA (ring vibrations are assigned via Wilson numbers).**

NRS acidic (cm <sup>-1</sup> )	NRS basic (cm <sup>-1</sup> )	SERS pH 4 (cm <sup>-1</sup> )	SERS pH 8 (cm <sup>-1</sup> )	assignments
2550				v (S-H)
1628		1700		v (C=O)
1575	1572	1560	1557	8b2
	1418		1421	v (O=C=O')
	1366		1378	v (O=C=O')
1162	1163	1144	1153	
1108	1108	1101	1100	
993	993	990	991	12a1 $\delta$ (ring)
934.3	898	858.4		
872.3		789.1		

$\delta$  = in plane deformation; v = stretch, NRS = normal Raman spectroscopy, SERS = surface enhanced Raman spectroscopy.

All SERS spectra reported in the following sections were obtained on nanoparticle probes where excess reporter molecules were removed by centrifugation at 5000 rpm, followed by resuspension in milli-Q water by sonication. Even though the SERS and normal Raman spectra (NRS) share similar features, there are certain spectral differences (see Figure 3) that indicate that the reporter is binding to the particle surface. The v(S-H) vibration found at 2550 cm<sup>-1</sup> that is present in acidic NRS of 3,5-DMBA is absent from the SERS spectra at pH 4. This is an indication that the reporter molecule's thiol groups are indeed binding to the Au surface. In the acidic NRS of 3,5-DMBA the v(C=O) vibration at 1628 cm<sup>-1</sup> (which is common for aromatic carboxylic acid) is shifted to 1700 cm<sup>-1</sup> in the SERS spectrum. This shift is common among aromatic carboxylic acids bound to metal nanoparticles.<sup>19, 24</sup> The enhancement factor for the vibration was calculated to be  $\sim 10^8$

based on the molecule's concentration and comparison to the regular Raman scattering signal of the molecule in solution (see Fig. 3).

The nanoparticle SERS pH probe was calibrated using a phosphate/citrate buffer at 5 discrete pH values on a glass cover slip. The smallest number of spectra collected at a single pH step was 322 spectra at pH 7, where each SERS spectrum was collected from a different position on the substrate. Each spectrum was normalized against the 12a1  $\delta(\text{ring})$  vibration. This vibration has a consistent SERS signal across the entire pH range reported here. The average SERS spectrum for each step as a function of pH is shown in Figure 4. Vibrational modes that are pH sensitive are clearly visible at 1700, 1420, 1380, and 870  $\text{cm}^{-1}$ . Peaks at 1700  $\text{cm}^{-1}$ , 1420  $\text{cm}^{-1}$ , and 1380  $\text{cm}^{-1}$  exhibit the most noticeable pH sensitivity. The signal strength of the  $\nu(\text{C}=\text{O})$  band of carboxylic acid at 1700  $\text{cm}^{-1}$  responds inversely proportional to the 1420 and 1380  $\text{cm}^{-1}$  as a function of pH. This means that a greater pH contrast can be obtained by using the ratio between the 1420 or 1380  $\text{cm}^{-1}$  and the 1700  $\text{cm}^{-1}$  vibrational mode. The vibrational peak assignments can be seen in Table 1. For this work we chose to use the ratio between the 1420  $\text{cm}^{-1}$  and 1700  $\text{cm}^{-1}$  bands to report pH contrast. We chose to use the mode at 1420  $\text{cm}^{-1}$  as opposed to the 1380  $\text{cm}^{-1}$  vibration because at low pH this band is still present and therefore its intensity can be used in a ratiometric evaluation (Figure 4) throughout the entire pH range reported here.

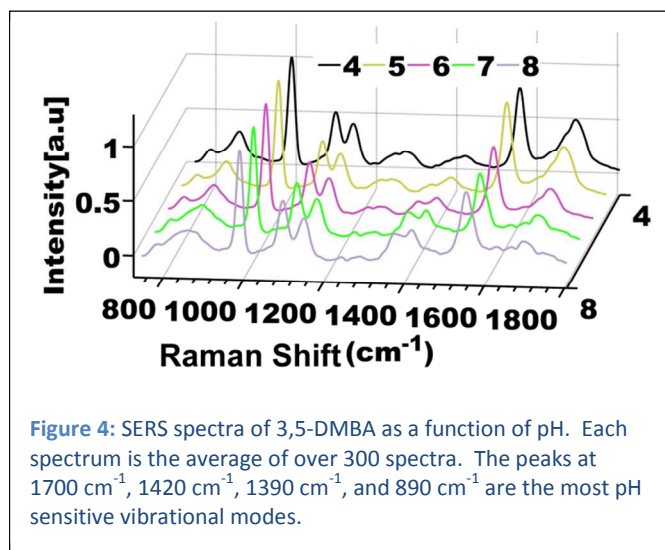


**Figure 4:** SERS spectra of 3,5-DMBA as a function of pH. Each spectrum is the average of over 300 spectra. The peaks at 1700  $\text{cm}^{-1}$ , 1420  $\text{cm}^{-1}$ , 1390  $\text{cm}^{-1}$ , and 890  $\text{cm}^{-1}$  are the most pH sensitive vibrational modes.

The ratio between the 1420  $\text{cm}^{-1}$  and 1700  $\text{cm}^{-1}$  vibration was evaluated at each pH for every spectrum (see Table 2). The total number of spectra measured at each pH step can be seen in column 2 of Table 2. To remove outliers, a Grubs test at 5% confidence was applied to the Raman peak ratios at each pH. In Table 2, column 3 we list the total number of data points that were remaining after applying the Grubs test. Of the 5 pH steps evaluated, the Grubs test rejected the most data collected at pH 4. Ten spectra were rejected after applying the Grubs test at pH 4, i.e. about 2.5% of the total data collected at this pH step. Precision is of major concern for accurate pH quantification. Considering the fact that each measurement was taken from different locations on the glass coverslip, a 2.5% rejection rate is remarkably small, indicating that this probe has excellent precision. The rejection percentages at pH 5, 6, 7, and 8 were 1.1%, 1.5%, 0%, and 0.14 %, respectively, which provides further evidence that 3,5-DMBA is very reliable as a pH-

sensitive SERS reporter. Spanning the physiological pH range is crucial for measuring alkalinity in vitro. Columns 1 through 4 with standard deviations from Table 2 are plotted in Figure 5.

**Table 2:** Statistics associated with standardization of the pH-sensing probe. The ratio and standard deviation referred to, here, is the peak intensity between the 1420 and 1700  $\text{cm}^{-1}$ . The visual representation can be seen in Figure 5.

pH	Initial number of data points	Number of data points after Grubbs test	Average ratio after Grubbs evaluations	Standard deviation after Grubbs evaluation
4	395	385	.2473	.0356
5	346	342	.3057	.0198
6	322	317	.5932	.0469
7	353	353	1.0475	.0988
8	705	704	1.3371	.0999

Grubs test was performed with a 5% confidence

A pH response curve was generated to fit our data using a Hill plot. Although the Hill plot generated an  $R^2$  value of .9997, the curve is used merely as a guide to the eye and is not used as a kinetic model. From this plot we can see that the pH resolution from pH 7 to 8 is 0.6 pH units and the resolution from pH 5 to 4 is 0.9 pH units. However, the best resolution is observed within the 5 to 7 pH range. In this region the resolution of our probe is approximately 0.34 pH units. A similarly high pH resolution

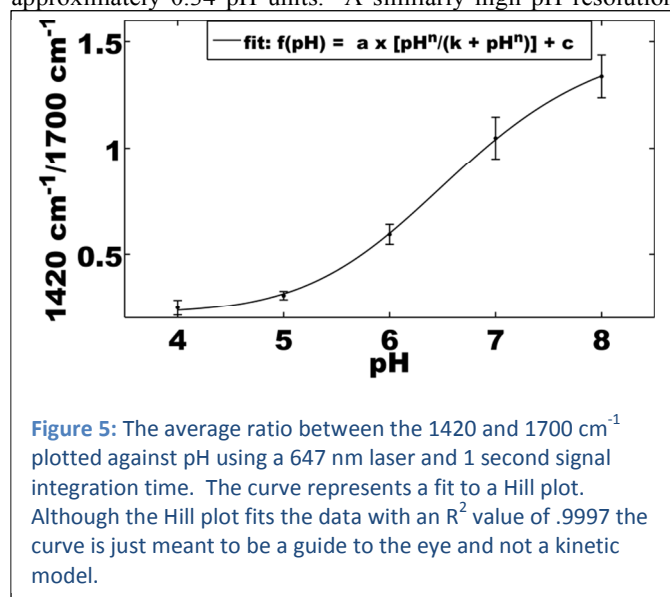


**Figure 5:** The average ratio between the 1420 and 1700  $\text{cm}^{-1}$  plotted against pH using a 647 nm laser and 1 second signal integration time. The curve represents a fit to a Hill plot. Although the Hill plot fits the data with an  $R^2$  value of .9997 the curve is just meant to be a guide to the eye and not a kinetic model.

has so far only been achieved by using hollow gold nanospheres (HGNS) or silica-core gold-shell nanospheres (SCGSNS) as a metal scaffold for a pH-sensitive SERS reporter.<sup>6, 8</sup> Although the HGNS and SCGSNS are metal structures that can stabilize SERS signals, both, HGNS and SCGSNS require multiple time-consuming synthesis and purification steps. As we have shown, our reporter system offers the same stability, however, using a simple and easily reproducible solid Au nanosphere.

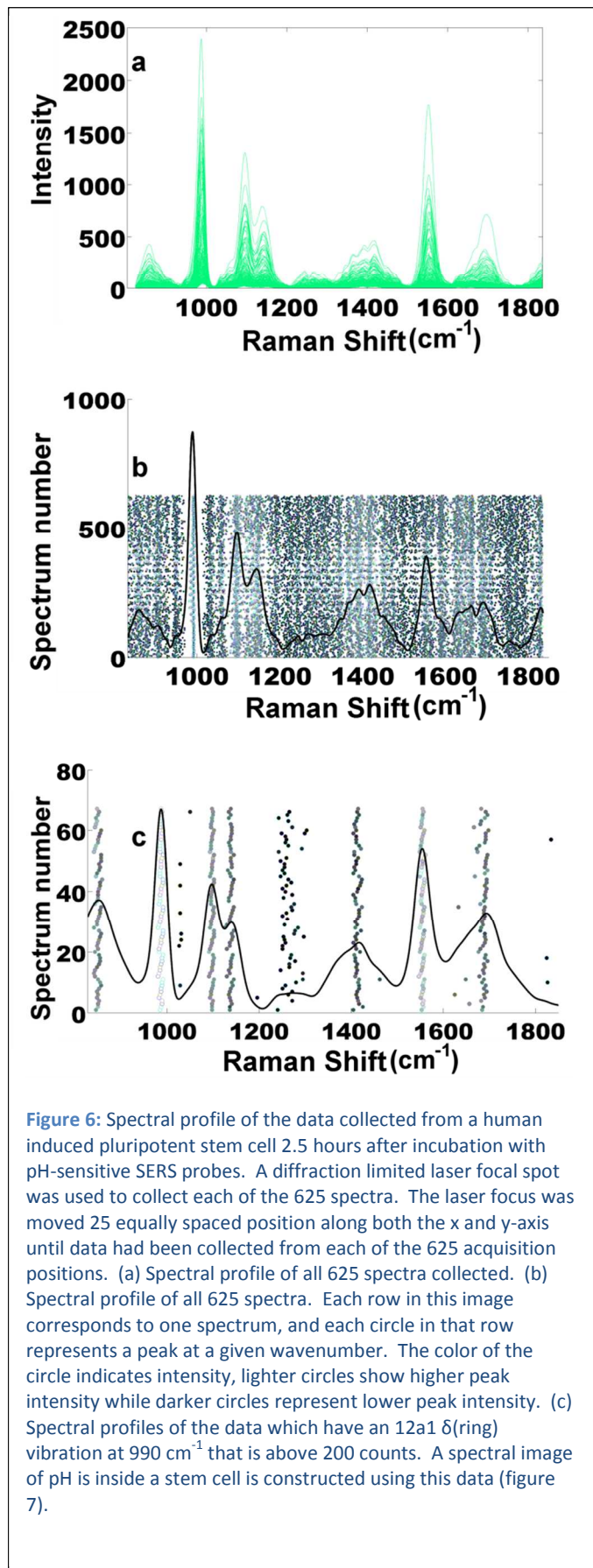


**Figure 6:** Spectral profile of the data collected from a human induced pluripotent stem cell 2.5 hours after incubation with pH-sensitive SERS probes. A diffraction limited laser focal spot was used to collect each of the 625 spectra. The laser focus was moved 25 equally spaced position along both the x and y-axis until data had been collected from each of the 625 acquisition positions. (a) Spectral profile of all 625 spectra collected. (b) Spectral profile of all 625 spectra. Each row in this image corresponds to one spectrum, and each circle in that row represents a peak at a given wavenumber. The color of the circle indicates intensity, lighter circles show higher peak intensity while darker circles represent lower peak intensity. (c) Spectral profiles of the data which have an 12a1  $\delta$ (ring) vibration at  $990\text{ cm}^{-1}$  that is above 200 counts. A spectral image of pH is inside a stem cell is constructed using this data (figure 7).

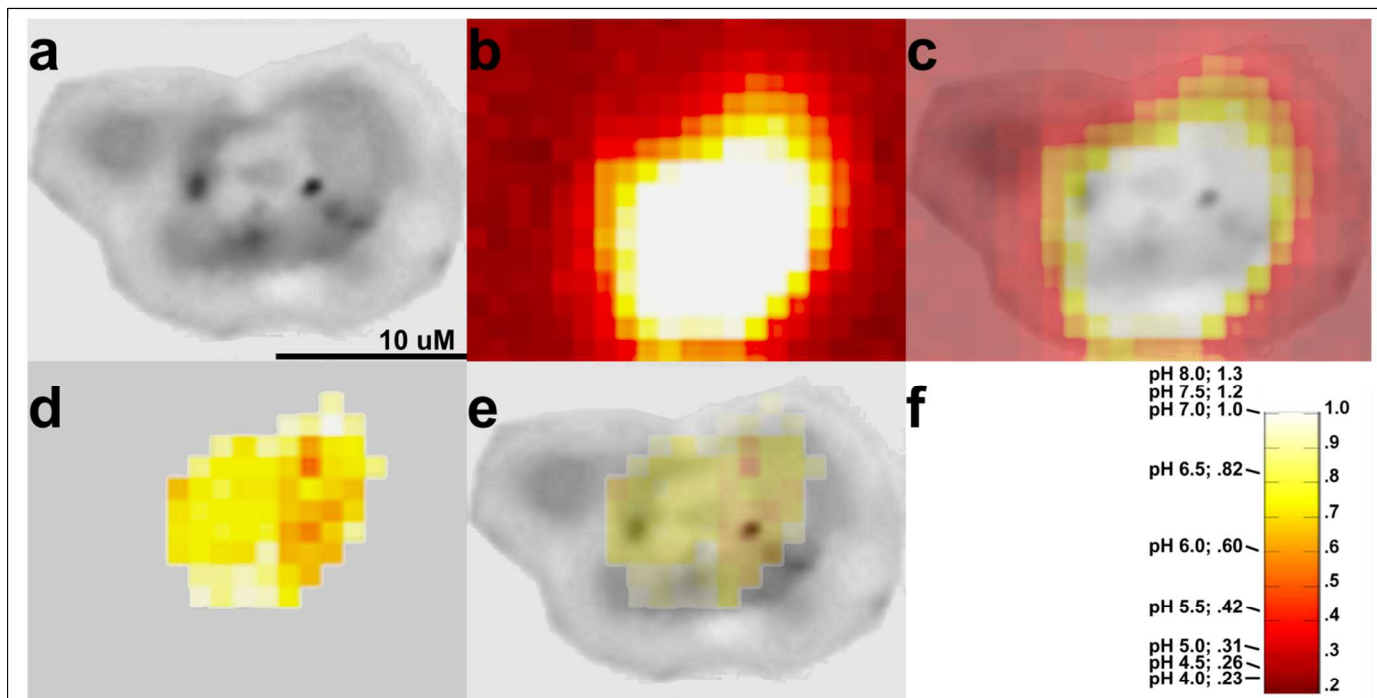
Lastly, the SERS probes were introduced to hiPSCs as described in the Materials and Methods section. A diffraction-limited laser spot scanned across 25 equally spaced positions along both the x and y axes was used to collect data from 625 different positions. This formed a  $25 \times 25$  square image grid that contained a single stem cell (see Figure 6 and Figure 7). Figure 6a shows the spectral profile for each of the 625 spectra in the image area after processing the data as performed for our standardization curve.

Figure 6a shows that most of the spectra have a similar profile as seen during the standardization experiments. Figure 6b is a more simplified version of Figure 6a. Each row shown in Figure 6b corresponds to a single spectrum, and each circle along that row is related to a peak being present in that spectrum at the corresponding wavenumber on the x-axis. From Figure 6b we can see highly conserved spectral regions that are indicative of the presence of the SERS probes. The black line in Figure 6b is the average spectral profile of all the 625 spectra collected. Figure 7a shows a widefield image of the hiPS cell. After collecting all the SERS spectra from the image plane, the peak intensity of the 12(a1)  $\delta$ (ring) vibration was used to reconstruct a SERS image of the cell's interior (Figure 7b). This peak yielded the most robust signal from the probe and thus was easily detectable. The reconstructed SERS image was then overlaid with the widefield image (Figure 7c) and both correspond well, highlighting the fact that the particles are indeed distributed throughout the cell. The ratio of the pH sensitive bands ( $1420\text{ cm}^{-1}$  and  $1700\text{ cm}^{-1}$ ) was also reconstructed into an image (Figure 7d), however, only the spectra in which the intensity of the 12a1  $\delta$ (ring) vibrational peak was above 200 counts (Figure 6c) were used to reconstruct this pH image. The colors in this image correspond to the ratio between the pH sensitive vibrations and the peak ratio can be translated into pH units by using Figure 7f. The deepest red spot in Figure 7d corresponds to a pH of 5.6 and the lightest colored spot corresponds to a pH of 6.9. SERS spectra corresponding to an acidic intracellular environment have previously been reported when nanoparticle reporters are taken up by the endocytosis pathway.<sup>15, 20</sup> The pH values inside endosomes range roughly between pH 5 and 6 in mammalian cells.<sup>36</sup> Late endosomes tend to approach the more acidic end of this range while early endosomes are only weakly acidic. Thus, the pH values reported by our probes are consistent with uptake into endosomes. Figure 7d and 7e also indicates that this acidic pH appears to be clustered near the center of the cell while less acidic profiles are located near the periphery of the cell. This is expected as the probes enter the cell from an almost neutral pH of the growth media, and are taken up into endosomes which become more acidic as they turn into late endosomes. Figure 7e is the superposition of the pH map with the image of our cell.

#### 4. Conclusion

We have demonstrated that 3,5-DMBA can serve as a colloidal linker for gold nanoparticles, turning them into an excellent pH reporter and SERS imaging probe. Although the specific mechanism through which our reporter creates hot spots needs further investigation, there is no doubt that the easily detectable SERS signals from our in vitro experiment are a direct result of our reporter's ability to induce and occupy SERS hot spots via the creation of multimeric aggregates. When the probes were introduced to hiPSCs the SERS signal was easily detectable against the cellular background and the pH-defining spectral peak ratios were readily obtained.

## ARTICLE



**Figure 7:** Spectral image of a live human induced pluripotent stem cell (hiPSC) after an 2.5hr incubation time with our pH-sensitive SERS probe. A diffraction limited laser (647 nm) focal spot was moved to 25 evenly spaced positions along both the x and y direction, where a 1 second integration time was used to collect data from each of the 625 spot positions. The spectral information was then used to construct the SERS images of a living stem cell. (a) A wide field image of the live hiPSC. (b) Spectral image of the SERS probe distribution inside the cell using only the intensity of the 12a1  $\delta$ (ring) vibration at  $990\text{ cm}^{-1}$  of the SERS probes. Lighter pixels signify a more intense 12a1  $\delta$ (ring) peak. (c) An overlay of the SERS image 'b' and the wide field image in 'a'. (d) Spectral image of pH distribution in a live hiPSC. This image was generated using the intensity ratio between the  $\nu(\text{O}=\text{C}=\text{O})$  and  $\nu(\text{C}=\text{O})$  peaks (at  $1420$  and  $1700\text{ cm}^{-1}$  respectively) from the SERS spectra collected. To ensure that measurements were from the laser focal plane, only SERS spectra that exhibited a 12a1  $\delta$ (ring) mode above a threshold intensity of 200 counts were used to map the pH. (e) Overlay of the pH-map 'd' and the wide field image 'a'. (f) Color map derived from the standardization curve (figure 5) of the pH-probe. The color map is used for figures 'd' and 'e'. The values on the left side of the color map are 1) the pH values from 4 to 8 in half unit increments followed by 2) the ratio of the pH deterministic peaks for those pH values. The values to the right of the color map correspond just to the ratio of the pH deterministic peaks.

Already 2.5 hrs after the introduction of our pH sensing probes to the cells a clear picture of the pH distribution emerges. Assuming that the intracellular pH of a stem cell changes as a function of their differentiation state this probe could serve as a valuable tool for studying stem cell differentiation, due to their robust and reliable pH signal. However, this probe is not limited to stem cell analysis. In pH detection the pH resolution determines how quickly a pH altering event can be detected. To our knowledge a highly reproducible pH resolution of 0.34 pH units is the best pH resolution achieved with regular gold nanoparticle SERS probes to date. It should be noted that this level of resolution is achieved with a simple gold colloidal scaffold and not HGNS or SiCAuNS which are known to yield better reproducible SERS signals and provide better pH resolution.<sup>6, 8</sup> Benzoic acid derivatives, such as 4-

Mercaptobenzoic acid have seen great success as pH reporters, however the best resolution achieved with unmodified commercially available compounds has been roughly 0.5 pH units. This resolution was achieved using HGNS, which reduced the signal fluctuations, and therefore improved the reporter's pH resolution.<sup>8</sup> Our reporter which is also a benzoic acid derivative has improved resolution without the need for designing and synthesizing higher order metal scaffolds. Furthermore, our probe is able to report pH over the entire physiological pH range and functions as an intracellular pH probe. Thus, 3,5-DMBA's ability to induce nanoparticle hotspots and maximize the SERS intensity not only aids in local pH-sensing but also in cellular imaging in general.

### Acknowledgements

We would like to thank Deborah K. Lieu (UC Davis) for providing and culturing the human induced pluripotent stem cells (hiPSCs) utilized in this study.

This work was supported by funding from the National Science Foundation. The Center for Biophotonics and an NSF Science and Technology Center, is managed by the University of California, Davis, under Cooperative Agreement No. PHY0120999.

## Notes and references

<sup>a</sup> NSF Center for Biophotonics Science and Technology, University of California, Davis, Sacramento, California 95817, United States.

<sup>b</sup> Department of Chemistry, University of California, Davis, Davis, California 95616, United States. Tel: +19167340688; llawson1@gmail.com.

<sup>c</sup> Department of Pathology and Laboratory Medicine, University of California, Davis, Sacramento, CA 95817, United States. Tel: +19167340774; E-mail: jwjchan@ucdavis.edu or james.chan@cbst.ucdavis.edu

<sup>d</sup> Department of Internal Medicine, University of California, Davis, Sacramento, California 95817, United States, and Department of Physics, University of Bielefeld, 33501 Bielefeld, Germany. Fax: +495211062958; Tel: +495211065451; E-mail: trhuser@ucdavis.edu or thomas.huser@physik.uni-bielefeld.de

1. G. Agel, W. Nultsch, EFFECTS OF GASSING, PH, QUENCHING AGENTS AND PHOTODYNAMICALLY ACTIVE COMPOUNDS ON PHOTOBLEACHING AND PHOTOINHIBITION OF THE CYANOBACTERIUM ANABAENA-VARIABILIS. *Archives of Microbiology* 1987, 149. 168-172, DOI: 10.1007/bf00425084.
2. D. M. Benson, J. Bryan, A. L. Plant, A. M. Gotto, L. C. Smith, DIGITAL IMAGING FLUORESCENCE MICROSCOPY - SPATIAL HETEROGENEITY OF PHOTOBLEACHING RATE CONSTANTS IN INDIVIDUAL CELLS. *J. Cell Biol.* 1985, 100. 1309-1323, DOI: 10.1083/jcb.100.4.1309.
3. K. W. Dunn, S. Mayor, J. N. Myers, F. R. Maxfield, APPLICATIONS OF RATIO FLUORESCENCE MICROSCOPY IN THE STUDY OF CELL PHYSIOLOGY. *Faseb J.* 1994, 8. 573-582.
4. J. Widengren, A. Chmyrov, C. Eggeling, P. A. Lofdahl, C. A. M. Seidel, Strategies to improve photostabilities in ultrasensitive fluorescence spectroscopy. *J. Phys. Chem. A* 2007, 111. 429-440, DOI: 10.1021/jp0646325.
5. C. L. Zavaleta, B. R. Smith, I. Walton, W. Doering, G. Davis, B. Shojaei, M. J. Natan, S. S. Gambhir, Multiplexed imaging of surface enhanced Raman scattering nanotags in living mice using noninvasive Raman spectroscopy. *Proceedings of the National Academy of Sciences of the United States of America* 2009, 106. 13511-13516, DOI: 10.1073/pnas.0813327106.
6. R. A. Jensen, J. Sherin, S. R. Emory, Single nanoparticle based optical pH probe. *Applied Spectroscopy* 2007, 61. 832-838.
7. S. Lee, H. Chon, M. Lee, J. Choo, S. Y. Shin, Y. H. Lee, I. J. Rhyu, S. W. Son, C. H. Oh, Surface-enhanced Raman scattering imaging of HER2 cancer markers overexpressed in single MCF7 cells using antibody conjugated hollow gold nanospheres. *Biosensors & Bioelectronics* 2009, 24. 2260-2263, DOI: 10.1016/j.bios.2008.10.018.

8. A. M. Schwartzberg, T. Y. Oshiro, J. Z. Zhang, T. Huser, C. E. Talley, Improving nanoprobe using surface-enhanced Raman scattering from 30-nm hollow gold particles. *Analytical Chemistry* 2006, 78. 4732-4736, DOI: 10.1021/ac060220g.
9. L. O. Brown, S. K. Doorn, A controlled and reproducible pathway to dye-tagged, encapsulated silver nanoparticles as substrates for SERS multiplexing. *Langmuir* 2008, 24. 2277-2280, DOI: 10.1021/la703853e.
10. T. Chen, H. Wang, G. Chen, Y. Wang, Y. H. Feng, W. S. Teo, T. Wu, H. Y. Chen, Hotspot-Induced Transformation of Surface-Enhanced Raman Scattering Fingerprints. *Acs Nano* 2010, 4. 3087-3094, DOI: 10.1021/nn100269v.
11. M. Moskovits, D. H. Jeong, Engineering nanostructures for giant optical fields. *Chemical Physics Letters* 2004, 397. 91-95, DOI: 10.1016/j.cpl.2004.07.112.
12. C. E. Talley, J. B. Jackson, C. Oubre, N. K. Grady, C. W. Hollars, S. M. Lane, T. R. Huser, P. Nordlander, N. J. Halas, Surface-enhanced Raman scattering from individual Au nanoparticles and nanoparticle dimer substrates. *Nano Letters* 2005, 5. 1569-1574, DOI: 10.1021/nl050928v.
13. K. L. Wustholz, A. I. Henry, J. M. McMahon, R. G. Freeman, N. Valley, M. E. Piotti, M. J. Natan, G. C. Schatz, R. P. Van Duyne, Structure-Activity Relationships in Gold Nanoparticle Dimers and Trimers for Surface-Enhanced Raman Spectroscopy. *Journal of the American Chemical Society* 2010, 132. 10903-10910, DOI: 10.1021/ja104174m.
14. P. H. C. Camargo, M. Rycenga, L. Au, Y. N. Xia, Isolating and Probing the Hot Spot Formed between Two Silver Nanocubes. *Angewandte Chemie-International Edition* 2009, 48. 2180-2184, DOI: 10.1002/anie.200806139.
15. J. Kneipp, H. Kneipp, M. McLaughlin, D. Brown, K. Kneipp, In vivo molecular probing of cellular compartments with gold nanoparticles and nanoaggregates. *Nano Letters* 2006, 6. 2225-2231, DOI: 10.1021/nl061517x.
16. A. Pallaoro, G. B. Braun, N. O. Reich, M. Moskovits, Mapping Local pH in Live Cells Using Encapsulated Fluorescent SERS Nanotags. *Small* 2010, 6. 618-622, DOI: 10.1002/sml.200901893.
17. G. B. Braun, S. J. Lee, T. Laurence, N. Fera, L. Fabris, G. C. Bazan, M. Moskovits, N. O. Reich, Generalized Approach to SERS-Active Nanomaterials via Controlled Nanoparticle Linking, Polymer Encapsulation, and Small-Molecule Infusion. *Journal of Physical Chemistry C* 2009, 113. 13622-13629, DOI: 10.1021/jp903399p.
18. T. A. Laurence, G. Braun, C. Talley, A. Schwartzberg, M. Moskovits, N. Reich, T. Huser, Rapid, Solution-Based Characterization of Optimized SERS Nanoparticle Substrates. *Journal of the American Chemical Society* 2009, 131. 162-169, DOI: 10.1021/ja806236k.
19. C. E. Talley, L. Jusinski, C. W. Hollars, S. M. Lane, T. Huser, Intracellular pH sensors based on surface-enhanced Raman scattering. *Analytical Chemistry* 2004, 76. 7064-7068, DOI: 10.1021/ac049093j.
20. J. Kneipp, H. Kneipp, B. Wittig, K. Kneipp, One- and two-photon excited optical pH probing for cells using surface-enhanced Raman and hyper-Raman nanosensors. *Nano Letters* 2007, 7. 2819-2823, DOI: 10.1021/nl071418z.
21. S. W. Bishnoi, C. J. Rozell, C. S. Levin, M. K. Gheith, B. R. Johnson, D. H. Johnson, N. J. Halas, All-optical nanoscale pH meter. *Nano Letters* 2006, 6. 1687-1692, DOI: 10.1021/nl060865w.

22. C. A. Lieber, A. Mahadevan-Jansen, Automated method for subtraction of fluorescence from biological Raman spectra. *Applied Spectroscopy* 2003, *57*, 1363-1367.
23. P. T. Corbett, J. K. M. Sanders, S. Otto\*<sup>[a]</sup>, Exploring the Relation between Amplification and Binding in Dynamic Combinatorial Libraries of Macrocyclic Synthetic Receptors in Water. *Chemistry: a European journal* 2008, *14*, 2153 - 2166.
24. L. Lawson, T. Huser, Synthesis and Characterization of a Disulfide Reporter Molecule for Enhancing pH Measurements Based on Surface-Enhanced Raman Scattering. *Anal. Chem.* 2012.
25. P. C. Lee, D. Meisel, ADSORPTION AND SURFACE-ENHANCED RAMAN OF DYES ON SILVER AND GOLD SOLS. *Journal of Physical Chemistry* 1982, *86*, 3391-3395.
26. F. R. Dollis, W. G. Fateley, F. F. Bentley. New York, p 111.
27. G. Socrates, in *Infrared and Raman Characteristic Group Frequencies*. John Wiley and Sons: Chichester, 3rd edn., 2001, p 132 and 136.
28. M. S. Newman, H. A. Karnes, CONVERSION OF PHENOLS TO THIOPHENOLS VIA DIALKYLTHIOCARBAMATES. *Journal of Organic Chemistry* 1966, *31*, 3980-&.
29. P. K. Jain, I. H. El-Sayed, M. A. El-Sayed, Au nanoparticles target cancer. *Nano Today* 2007, *2*, 18-29.
30. S. Link, M. A. El-Sayed, Size and temperature dependence of the plasmon absorption of colloidal gold nanoparticles. *Journal of Physical Chemistry B* 1999, *103*, 4212-4217.
31. J. K. Lim, O. Kwon, S. W. Joo, Interfacial structure of 1,3-benzenedithiol and 1,3-benzenedimethanethiol on silver surfaces: Surface-enhanced Raman scattering study and theoretical calculations. *Journal of Physical Chemistry C* 2008, *112*, 6816-6821, DOI: 10.1021/jp077409w.
32. J. K. Lim, Y. Kim, O. Kwon, S. W. Joo, Adsorption of 1,3-benzenedithiol and 1,3-benzenedimethanethiol on gold surfaces. *Chemphyschem* 2008, *9*, 1781-1787, DOI: 10.1002/cphc.200800175.
33. O. C. Compton, F. E. Osterloh, Evolution of size and shape in the colloidal crystallization of gold nanoparticles. *Journal of the American Chemical Society* 2007, *129*, 7793-7798, DOI: 10.1021/ja069033q.
34. J. Y. Shim, V. K. Gupta, Reversible aggregation of gold nanoparticles induced by pH dependent conformational transitions of a self-assembled polypeptide. *Journal of Colloid and Interface Science* 2007, *316*, 977-983, DOI: 10.1016/j.jcis.2007.08.021.
35. J. H. Yoon, J. S. Park, S. Yoon, Time-Dependent and Symmetry-Selective Charge-Transfer Contribution to SERS in Gold Nanoparticle Aggregates. *Langmuir* 2009, *25*, 12475-12480, DOI: 10.1021/la9031865.
36. M. Grabe, G. Oster, Regulation of organelle acidity. *Journal of General Physiology* 2001, *117*, 329-343, DOI: 10.1085/jgp.117.4.329.